Electronic supplementary information

Stabilizing high-voltage $LiNi_{0.5}Mn_{1.5}O_4$ cathode towards all solid state battery: a Li-Al-Ti-P-O solid electrolyte nano-shell with host material

Li Li,[a] Rui Zhao,[a] Tinghua Xu,[a] Dandan Wang,[a] Du Pan,[a] Xia Lu,[c] Guanjie He,[d] Kun Zhang,[a] Caiyan Yu[b] and Ying Bai*[a]*

[a] School of Physics & Electronics, Henan University, Kaifeng 475004, P.R. China.

[b] National Demonstration Center for Experimental Physics and Electronics Education, School of Physics and Electronics, Henan University, Kaifeng 475004, PR China.

[c] School of Materials, Sun Yat-sen University, Guangzhou 510275, P.R. China.

[d] Materials Research Centre, UCL Department of Chemistry, Christopher Ingold Building, 20 Gordon Street, London, WC1H 0AJ, UK.

E-mail: ybai@henu.edu.cn (Ying Bai); cyyu@henu.edu.cn (Caiyan Yu)

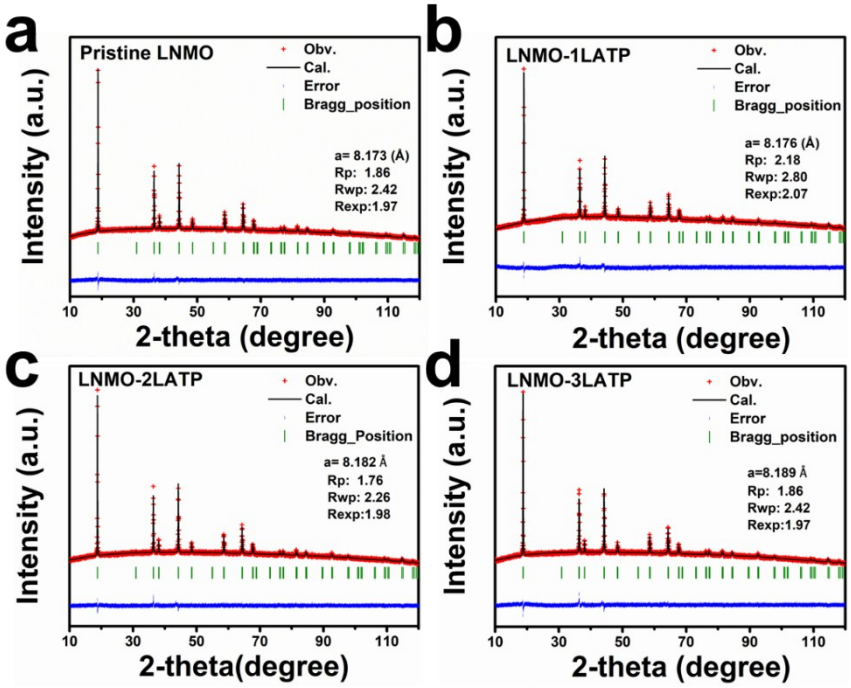

Fig. S1 Refinement XRD patterns of (a) pristine LNMO, (b) LNMO-1LATP, (c) LNMO-2LATP and (d) LNMO-3LATP.

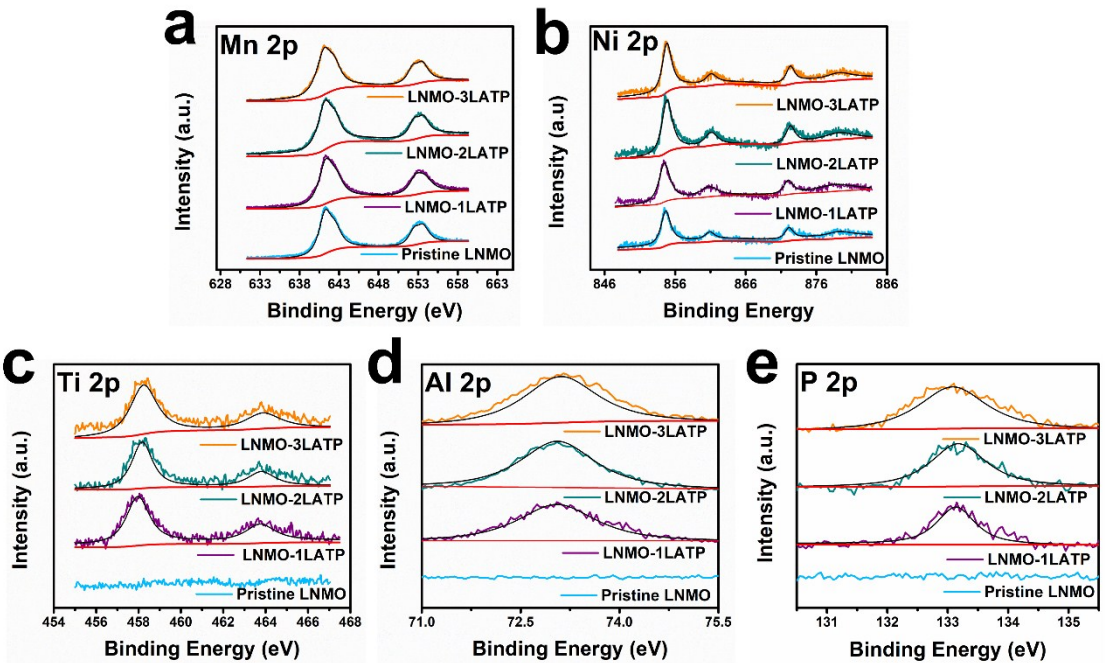

Fig. S2 XPS results of (a) Mn 2p, (b) Ni 2p, (c) Ti 2p, (d) Al 2p and (e) P 2p of all samples.

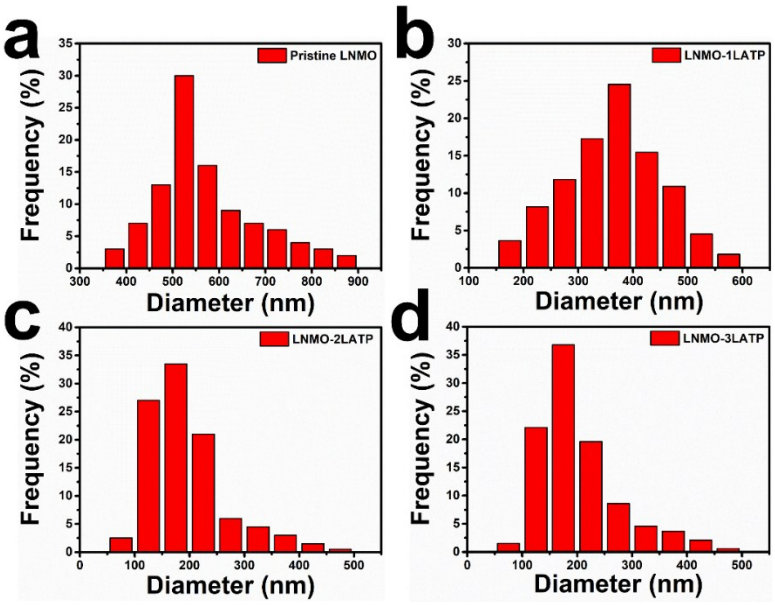

Fig. S3 Particle size distribution of (a) pristine LNMO, (b) LNMO-1LATP, (c) LNMO-2LATP and (d) LNMO-3LATP.

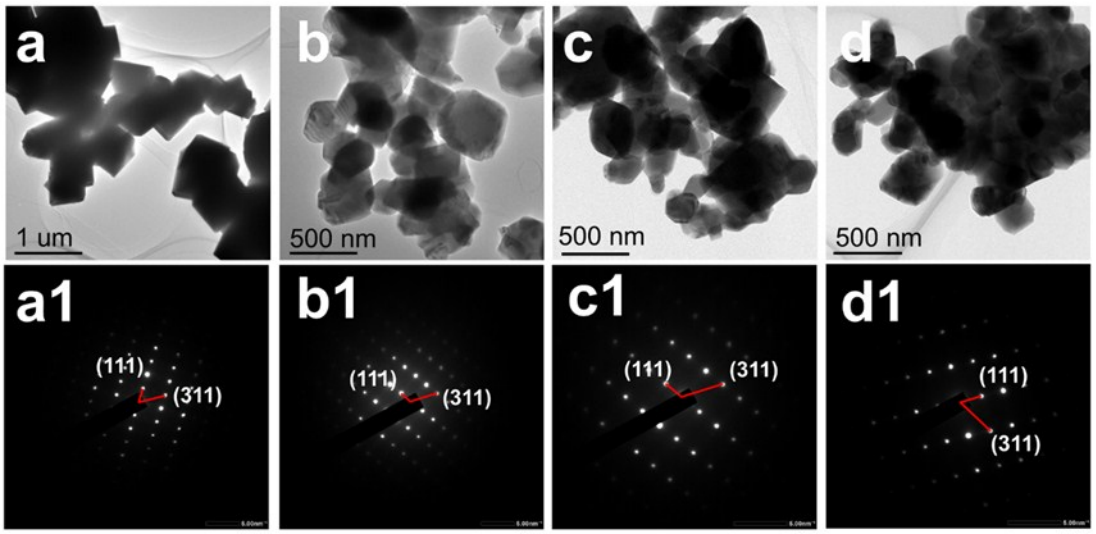

Fig. S4 The TEM images (a-d) and selected area electron diffraction patterns (a_1-d_1) of (a) Pristine-LNMO, (b) LNMO-1LATP, (c) LNMO-2LATP and (d) LNMO-3LATP.

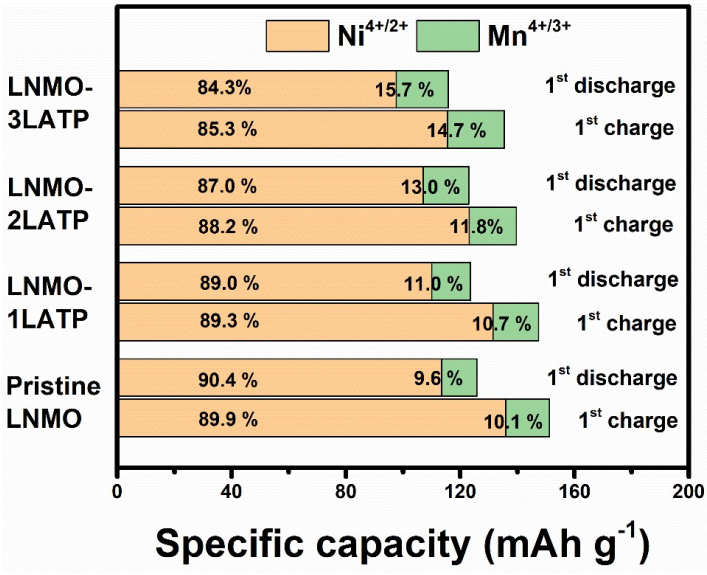

Fig. S5 Specific capacity contributions of $Ni^{4+/2+}$ and $Mn^{4+/3+}$ calculated from the initial charge-discharge voltage profiles in Fig. 5a.

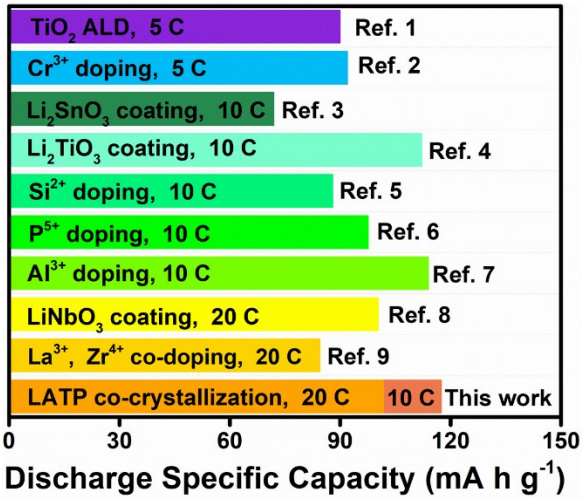

Fig. S6 Comparison of the rate performances among this work and previously reported LNMO cathodes.

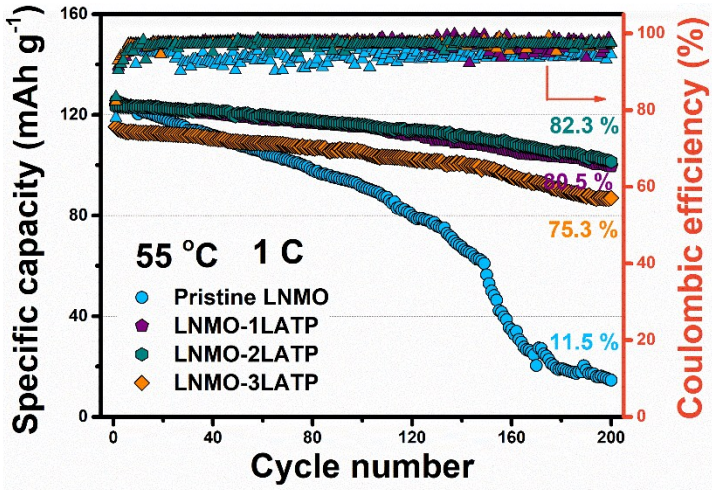

Fig. S7 Cycling performances of all samples at 1 C with corresponding coulombic efficiencies (tested at 55 °C).

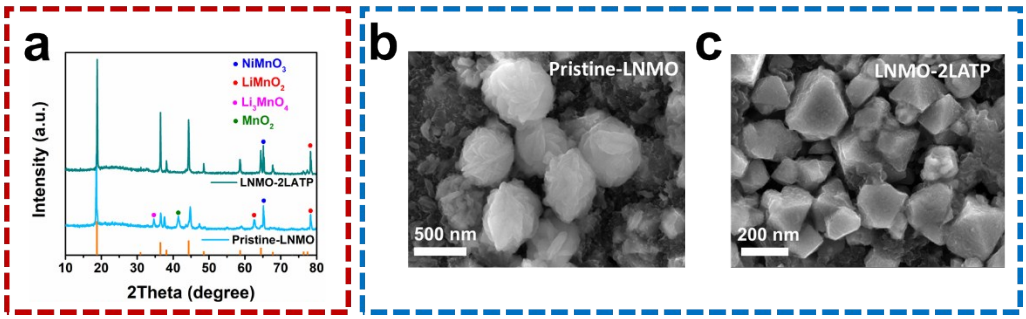

Fig. S8 (a) XRD pattern and (b-c) SEM images of pristine LNMO and LNMO-2LATP samples after 100 cycles at 55°C.

In Fig. S8a, the densities of {111}, {311} and {400} diffraction peaks of the pristine sample are sharply declined, and meanwhile some peaks are disappeared or broadened. Additionally, a significant peak shift of the spinel phase toward lower angles and some new phase ($NiMnO_3$, $LiMnO_2$, Li_3MnO_4 and MnO_2) can be detected, which indicates a lattice expansion and a serious decomposition of LNMO. As for the LNMO-2LATP sample, all diffraction peaks of LNMO can still be detected, besides the $NiMnO_3$ and $LiMnO_2$ also can be identified. These results indicated the structure collapse of LNMO after high-temperature cycling (100 cycles, 55 °C), and can be further proved by the SEM images in Fig. S8b-c. It is clear that the morphology of the pristine particle is seriously deteriorated, which is usually related to a dense CEI layer and the drastic attack of HF from the electrolyte. Moreover, the exposed surface of the pristine LNMO particles can accelerate the dissolution of TM ions at the elevated temperature.

Table S1 XRD refinement results of LNMO before and after modification.

Sample	a (Å)	Cell volume (Å3)	Rp (%)
Pristine LNMO	8.173(6)	546.0(5)	1.84
LNMO-1LATP	8.176(3)	546.6(1)	2.18
LNMO-2LATP	8.182(2)	547.7(8)	1.76
LNMO-3LATP	8.189(6)	549.2(7)	1.86

Table S2 Redox parameters of all samples.

Electrode	Redox	Redox potential (V)	D-Value (V)	FWHM
Pristine-LNMO	Ni^{2+}/Ni^{3+}	4.692/4.657	0.035	0.0305
	Ni^{3+}/Ni^{4+}	4.749/4.719	0.030	0.0239
LNMO-1LATP	Ni^{2+}/Ni^{3+}	4.701/4.680	0.021	0.0249
	Ni^{3+}/Ni^{4+}	4.764/4.734	0.030	0.0208
LNMO-2LATP	Ni^{2+}/Ni^{3+}	4.701/4.683	0.018.	0.0234
	Ni^{3+}/Ni^{4+}	4.764/4.737	0.027	0.0199
LNMO-3LATP	Ni^{2+}/Ni^{3+}	4.704/4.678	0.026	0.0402
	Ni^{3+}/Ni^{4+}	4.776/4.739	0.035	0.0249

FWHM: FWHM of reduction peaks.

	R_s (Ω)			R_{sf} (Ω)			R_{ct} (Ω)		
	1st	30th	60th	1st	30th	60th	1st	30th	60th
Pristine-LNMO	2.02	3.57	6.68	247	466	643	342	647	832
LNMO-2LATP	1.69	2.96	5.57	212	286	350	316	523	648

Table S3. The impedance values of the pristine and LNMO-2LATP cathodes.

Supplementary References

1. B. Xiao, H. Liu, J. Liu, Q. Sun, B. Wang, K. Kaliyappan, Y. Zhao, M. N. Banis, Y. Liu, R. Li, T. K. Sham, G. A. Botton, M. Cai and X. Sun, Adv. Mater., 2017, **29**, 1703764.
2. J. Wang, P. Nie, G. Y. Xu, J. M. Jiang, Y. T. Wu, R. R. Fu, H. Dou and X. G. Zhang, *Adv. Funct. Mater.*, 2018, **28**, 1704808.
3. J. Mou, Y. L. Deng, Z. C. Song, Q. J. Zheng, K. H. Lam and D. M. Lin, *Dalton. Trans.*, 2018, **47**, 7020-7028.
4. J. S. Park, X. Meng, J. W. Elam, S. Hao, C. Wolverton, C. Kim and J. Cabana, *Chem. Mater.*, 2014, **26**, 3128-3134.
5. S. Nageswaran, K. Miriam, S. J. Kin and M. Srinivasan, *J. Power Sources*, 2017, **346**, 89-96.
6. Y. F. Deng, S. X. Zhao, Y. H. Xu, K. Gao and C. W. Nan, *Chem. Mater.*, 2015, **27**, 7734-7742.
7. G. B. Zhong, Y. Y. Wang, Z. C. Zhang and C. H. Chen, *Electrochim. Acta*, 2011, **56**, 6554-6561.
8. H. Kim, D. Byun, W. Chang, H. G. Jung and W. Choi, *J. Mater. Chem. A*, 2017, **5**, 25077-25089.
9. W. Liu, Q. Shi, Q. Qu, T. Gao, G. Zhu, J. Shao and H. Zheng, *J. Mater. Chem. A*, 2017, **5**, 145-154.